

## Subseasonal Prediction of Land Cold Extremes in Boreal Wintertime

Baoqiang Xiang<sup>1,2</sup> , Y. Qiang Sun<sup>1,3</sup> , Jan-Huey Chen<sup>1,2</sup> , Nathaniel C. Johnson<sup>1</sup> , and Xianan Jiang<sup>4</sup> 

<sup>1</sup>NOAA/Geophysical Fluid Dynamics Laboratory, Princeton, NJ, USA, <sup>2</sup>Cooperative Programs for the Advancement of Earth System Science, University Corporation for Atmospheric Research, Boulder, CO, USA, <sup>3</sup>Program in Atmospheric and Oceanic Sciences, Princeton University, Princeton, NJ, USA, <sup>4</sup>Joint Institute for Regional Earth System Science and Engineering, University of California, Los Angeles, CA, USA

### Key Points:

- The wintertime land extreme cold days can be largely predicted by the ECMWF model 2–4 weeks in advance
- The physical basis in predicting ECDs is mainly rooted in predicting a small subset of leading EOF modes of ECDs identified from observation
- The predictability source for the leading EOF modes originates from atmospheric internal modes and the land-atmosphere coupling

### Supporting Information:

- Supporting Information S1

### Correspondence to:

B. Xiang,  
baoqiang.xiang@noaa.gov

### Citation:

Xiang, B., Sun, Y. Q., Chen, J.-H., Johnson, N. C., & Jiang, X. (2020). Subseasonal prediction of land cold extremes in boreal wintertime. *Journal of Geophysical Research: Atmospheres*, 124, e2020JD032670. <https://doi.org/10.1029/2020JD032670>

Received 25 FEB 2020

Accepted 22 MAY 2020

Accepted article online 11 JUN 2020

**Abstract** Subseasonal climate prediction has emerged as a top forecast priority but remains a great challenge. Subseasonal extreme prediction is even more difficult than predicting the time-mean variability. Here we show that the wintertime cold extremes, measured by the frequency of extreme cold days (ECDs), are skillfully predicted by the European Centre for Medium-Range Weather Forecasts (ECMWF) model 2–4 weeks in advance over a large fraction of the Northern Hemisphere land region. The physical basis for such skill in predicting ECDs is primarily rooted in predicting a small subset of leading empirical orthogonal function (EOF) modes of ECDs identified from observations, including two modes in Eurasia (North Atlantic Oscillation and Eurasia Meridional Dipole mode) and three modes in North America (North Pacific Oscillation, Pacific-North America teleconnection mode, and the North America Zonal Dipole mode). It is of interest to note that these two modes in Eurasia are more predictable than the three leading modes in North America mainly due to their longer persistence. The source of predictability for the leading EOF modes mainly originates from atmospheric internal modes and the land-atmosphere coupling. All these modes are strongly coupled to dynamically coherent planetary-scale atmospheric circulations, which not only amplify but also prolong the surface air temperature anomaly, serving as a source of predictability at subseasonal timescales. The Eurasian Meridional Dipole mode is also tied to the lower-boundary snow anomaly, and the snow-atmosphere coupling helps sustain this mode and provides a source of predictability.

## 1. Introduction

At the frontier of climate forecasting, subseasonal prediction (usually referring to the timescales between 2 weeks and one season) has become an increasingly active research topic in recent years that has followed the rapidly growing societal demands for forecast products at these timescales. As a bridge to link the weather and seasonal climate prediction, subseasonal prediction is fraught with the challenges lying at the limits of deterministic weather and probabilistic climate prediction. As an initial value problem, short-range weather prediction largely depends on the accuracy of atmospheric initial conditions. In contrast, the skill for seasonal prediction is primarily attributed to the boundary forcing as a boundary value problem. Subseasonal prediction, which lies in between as a mixed initial and boundary value problem, is usually less skillful than both the weather and seasonal prediction. The grand challenge for this timescale is that the initial memory from the atmosphere is gradually lost (after around 10 days) while it only marginally benefits from the boundary forcing effect (White et al., 2017).

Despite this challenge, considerable progress has been achieved in the past decade, benefited partly from modeling advances as well as our improved knowledge of predictability sources. Meanwhile, this progress has been accelerated by some multiagency and international projects. For example, the World Weather Research Programme (WWRP) and World Climate Research Programme (WCRP) Subseasonal to Seasonal Prediction Project (S2S) is a multi-institutional effort to promote the subseasonal to seasonal predictions (Vitart et al., 2016), and initiatives, such as the NOAA/Modeling, Analysis, Predictions and Projections (MAPP) Program S2S Prediction Task Force, are providing a framework for needed weather–climate community interactions (Mariotti et al., 2018). The Subseasonal Experiment (SubX) is one of the projects targeting the S2S prediction participating in the NOAA/MAPP S2S Prediction Task Force (Pegion et al., 2019).

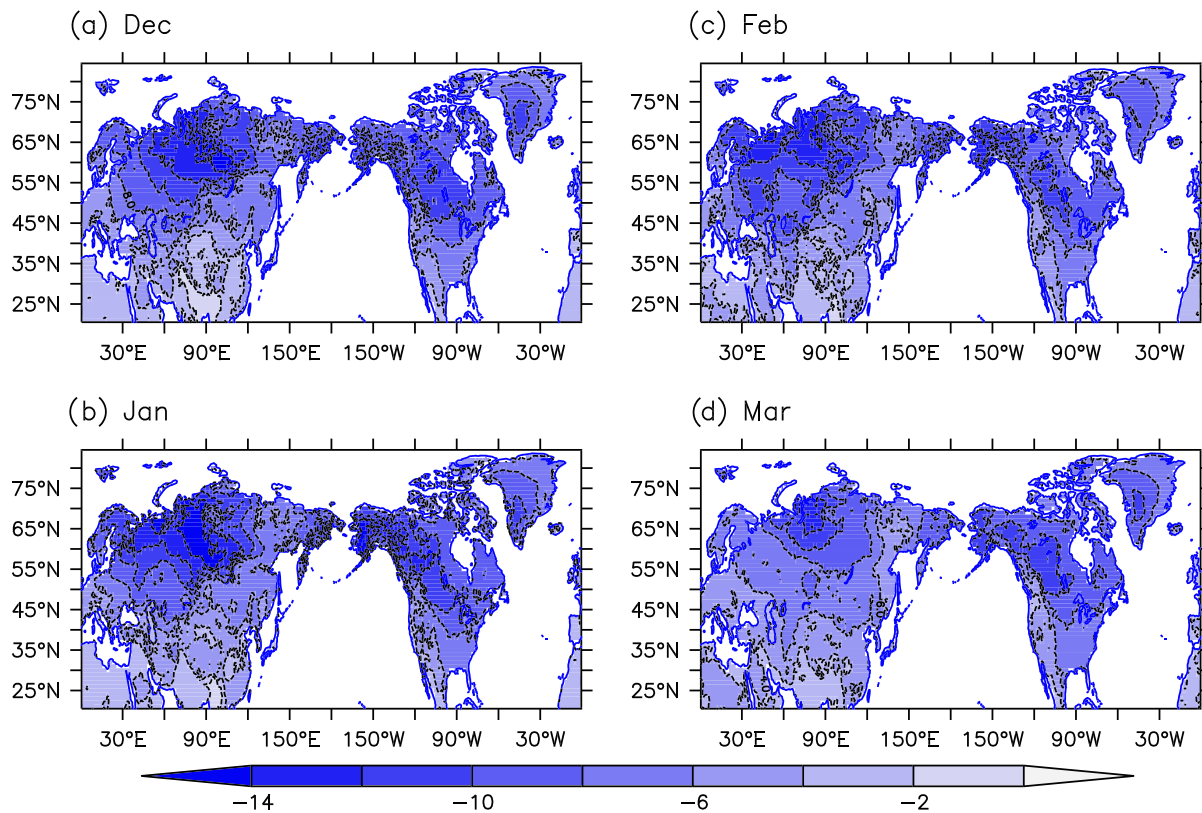


**Figure 1.** Observational temperature anomaly threshold for extreme cold days (K) from December to March. Note that the daily threshold is defined using the 21-calendar day window over 20 years (1997–2016).

In recent years, scientific interest in the subseasonal prediction has exploded, and some useful skill in predicting environmental variables has been extensively reported, for example, surface air temperature (Liang et al., 2018; Lin, 2018; Xiang et al., 2018; Yoo et al., 2018), precipitation (de Andrade et al., 2019), and Arctic sea ice (Wayand et al., 2019; Zampieri et al., 2018). The prediction of extreme departures from normal conditions lies at the forefront of emerging subseasonal forecast challenges, as such events result in the highest impacts on both societies and ecosystems. The prediction of extremes is generally more difficult than the prediction of time-mean variability. Recent literature reveals some limited but encouraging subseasonal extreme prediction results in forecasting tropical cyclones (Gao et al., 2019; Jiang et al., 2018; Lee et al., 2018; Xiang et al., 2014), heat waves (Batté et al., 2018; Dirmeyer et al., 2019; Ford et al., 2018), extreme rainfall/floods (Lee et al., 2017; Lin et al., 2018), and atmospheric rivers (Baggett et al., 2017; DeFlorio et al., 2018; Mundhenk et al., 2018).

The wintertime cold temperature extremes, usually caused by an incursion of cold polar air, are often accompanied by heavy snowfall and/or freezing precipitation. They have a tremendous influence on socioeconomic and human activities over large areas of heavily populated continents. Intriguingly, the occurrence frequency of wintertime cold extremes has increased in many land regions during the recent two decades despite the rise of global mean temperature (Cohen et al., 2020; Gong & Ho, 2004; Johnson et al., 2018; Park et al., 2011). The land cold extremes also experience pronounced subseasonal variations, which are linked to a number of drivers such as the Arctic Oscillation and Siberian High (Gong & Ho, 2004) and Madden-Julian Oscillation (MJO) (Jeong et al., 2005). A successful prediction of such extreme events several weeks ahead has immense socioeconomic benefits for effective hazard preparedness and risk management. Notwithstanding the great impacts of cold extremes, efforts toward understanding its prediction and predictability at subseasonal timescale have not garnered much attention. To the best of our knowledge, this is the first study aiming to systematically investigate this issue.

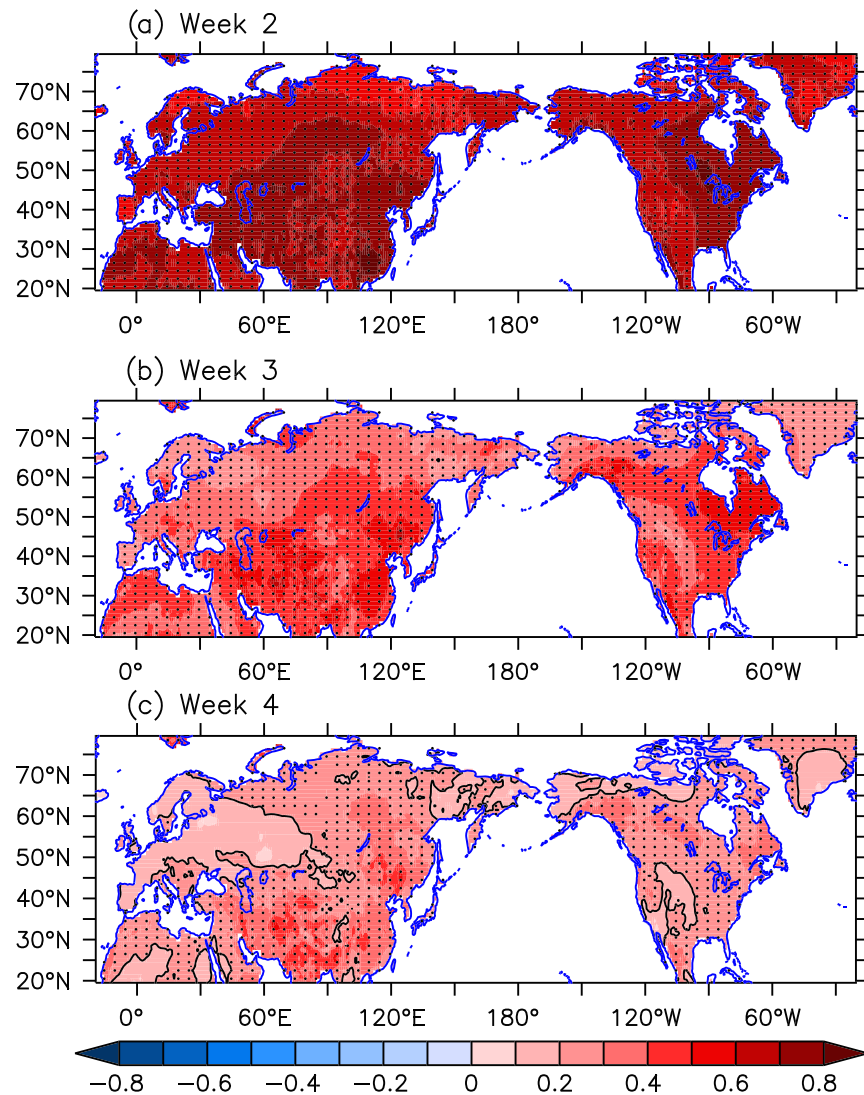


**Figure 2.** Correlation skill of weekly mean surface air temperature (SAT) from week 2 to week 4. The dots denote the region with the correlation skill significant at the 5% significance level, and the contours represent the correlation coefficient of 0.2.

The objective of this study is twofold. First, we aim to unravel the predominant physical mechanisms controlling the subseasonal variation of wintertime land cold extremes from observations, measured by one of the metrics: extreme cold days (ECDs). The second is to probe the predictability of ECDs in current state-of-the-art models, by examining the European Centre for Medium-Range Weather Forecasts (ECMWF) model that participated in the WWRP/WCRP S2S project (Vitart et al., 2016).

## 2. Data and Methodology

### 2.1. Observational and Hindcast Data

We analyze observational data that consist of the hourly ECMWF ERA5 reanalysis data (C3S, 2017) (surface air temperature, 500 hPa geopotential height, and snow albedo) and daily snow cover data from the National Ice Center's Interactive Multisensor Snow and Ice Mapping System (IMS) (National Ice Center, 2008). We also analyze forecast data derived from the ECMWF hindcast data sets using the Ensemble Prediction System (EPS), which are archived from the WWRP/WCRP S2S Prediction Project science plan (Vitart et al., 2016). Hindcasts are carried out twice per week (the start date remains the same for each year) with

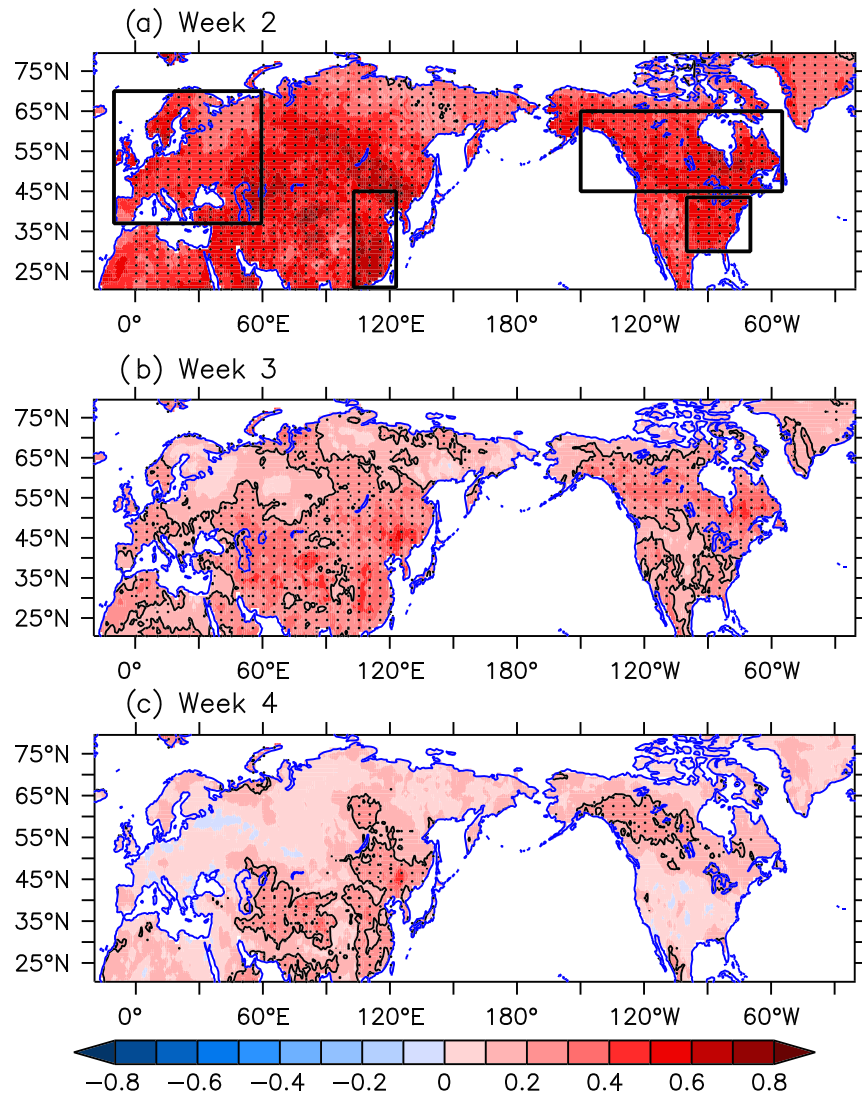


**Figure 3.** Similar to Figure 2 but for the correlation skill of weekly extreme cold days (ECDs). The ECD prediction over the four individual domains outlined in panel a) is further investigated in Figure 14.

11 ensemble members and 46 days integration. For the hindcast data, we analyze the cases initialized from December to February (DJF), while for observations, we focus on the period between December and March (DJFM), as some forecast data initialized on January and February extend to the ensuing March. The studied period covers 1997 to 2017 for both observations and model hindcasts, and there are 500 cases for hindcasts in total. We refer to seasons corresponding to the Northern Hemisphere.

## 2.2. Methodology

Similar to Xiang et al. (2018), the anomalous fields for observations are obtained by removing the time-mean and first four harmonics of the climatological annual cycle from the observational daily mean data. To correct for biases owing to model drift, the hindcast anomalies are calculated by removing the hindcast climatology as a function of hindcast starting date and lead time. Note that the interannual and even longer timescale variation is retained here.

Following Luo and Wang (2017), the extreme cold event is defined when the surface air temperature (SAT) anomalies are equal to or exceed the threshold of the 10th percentile of the descending sorted daily mean SAT anomalies. Considering the relatively small sample size in observations, we use a time window of 21 days centered at the specific day to define the threshold. For example, the calculation of the threshold

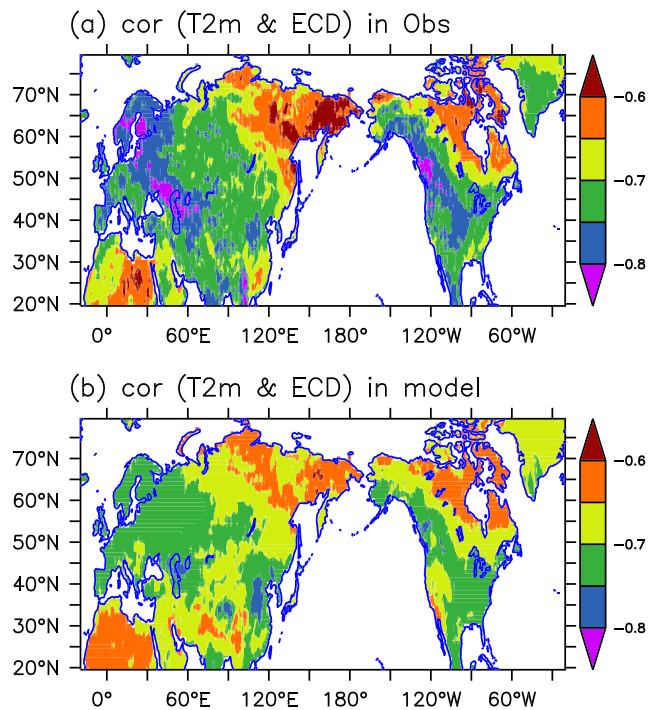


**Figure 4.** The simultaneous correlation coefficient between weekly mean SAT anomaly and weekly ECD anomaly in (a) observations and (b) model hindcast at week 3.

on 1 January is based on 20 years of SAT anomaly data within the time window between 22 December and 11 January. For model hindcasts, we use the ensemble-mean temperature anomalies with nine hindcast cases centered on a particular date to determine the threshold. For example, the threshold on 1 January is derived from cases initialized on the time window between 18 December and 11 January (18 December, 21 December, 25 December, 28 December, 1 January, 4 January, 8 January, and 11 January).

The impact of climate change on extreme cold events is not specifically evaluated here while its contribution is substantially smaller compared to the subseasonal and interannual variations. Consistently, there is no statistically significant trend variability of ECDs during the studied 20-year period from a Northern Hemisphere perspective (Johnson et al., 2018).

In this study, we assess the skill of deterministic ECD forecasts with the correlation coefficient, with the weekly data serving as the basis for all following analyses. To assess the significance of the anomalous correlation, we use the effective sample size calculated by considering the autocorrelation in the observed and forecast data (Bretherton et al., 1999; Yang et al., 2012).

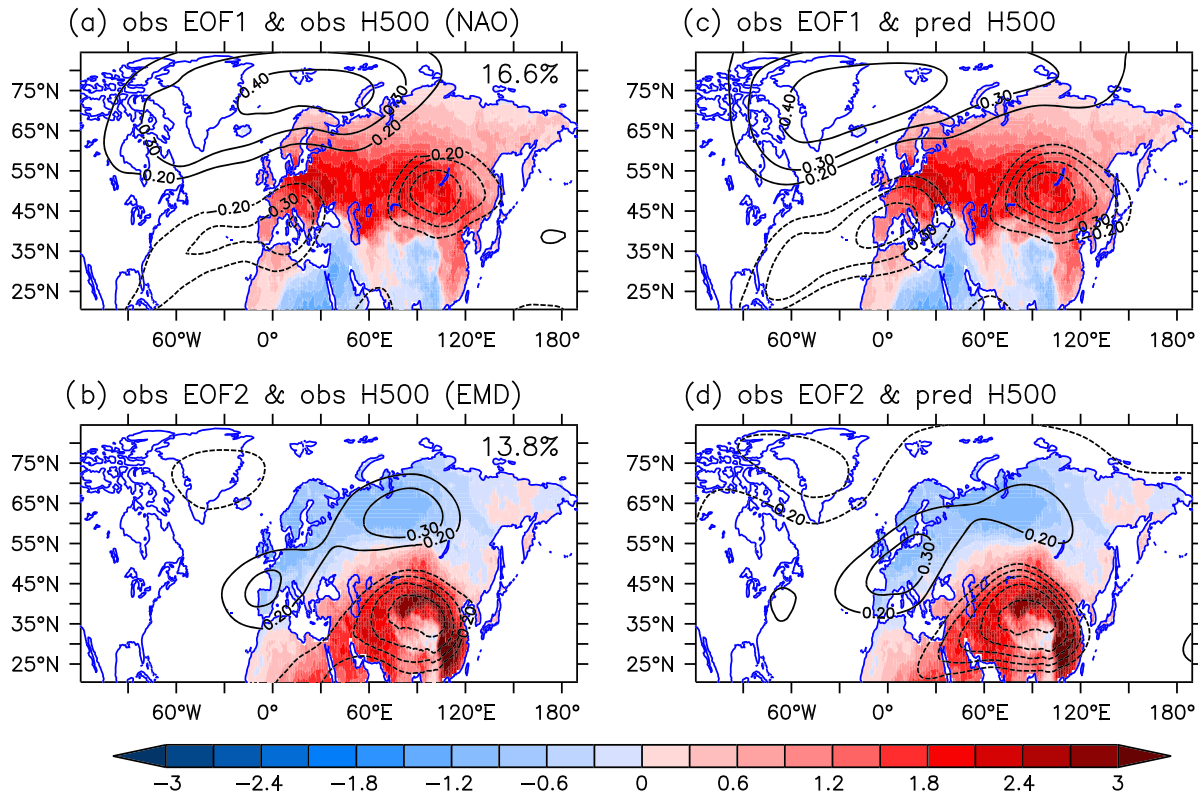
### 3. Results

Figure 1 illustrates the prominent spatial variation of monthly mean thresholds of observational SAT anomalies for defining ECDs. Compared to the low latitudes, the high latitudes, especially the interior continental regions, generally have a lower threshold (much colder temperature anomalies), including northern Eurasia (around  $-14$  K), Canada, and Alaska (around  $-10$  K). The threshold in North America features large zonal contrasts, with a lower threshold in the east than the west for the United States but with an opposite zonal contrast for Canada. The thresholds in March generally have a smaller amplitude (higher temperature anomalies) when comparing to the early months, reflecting a reduction in temperature variance despite a very similar pattern with the other months. Note that the threshold in model hindcasts derived from the ensemble-mean hindcasts varies with calendar date and also forecast lead time (Figure S1 in the supporting information). The threshold varies with forecast lead time since the variance of the ensemble-mean SAT anomalies generally decreases with the forecast lead time along with the decrease of signal to noise ratio (Figure S1). However, the threshold remains nearly unchanged after leaving 1 year out and is not sensitive to a minor change of the size of the time window.

#### 3.1. Overall Skill in Predicting SAT and ECD Anomalies

Before discussing the ECD forecasts, we first examine the skill in predicting weekly mean SAT in the Northern Hemisphere extratropical continents (Figure 2). Most of the land regions show significant week 2–4 (predictions at 2–4 weeks in advance) correlation skills in predicting SAT, except the regions in the western United States and Europe for the week 4 prediction. Compared to the mean SAT prediction, the weekly ECD (the occurrence frequency of ECD in a week) predictions exhibit a strikingly similar but overall lower correlation skill (Figure 3). Relatively high prediction skill is confined to a large area of China and Canada, where skill is significant even at week 4 (Figure 3c). Actually, the variations of weekly ECDs are highly correlated with the weekly mean SAT for both observations and model hindcasts with a correlation coefficient of about  $-0.6$  to  $-0.8$  (Figure 4). Thus, we can infer that about 40–60% of the variance of the weekly ECD frequency is attributed to the fluctuation of weekly mean SAT (the shift of the probability distribution function) so that the prediction skill of ECDs arises partially from the prediction of weekly mean SAT.

Why do some regions have more skill than others, and what are the climate conditions that promote elevated forecast skill in those regions? Addressing these questions is critical as they may provide guidance on identifying the windows of opportunity for generating useful subseasonal forecasts, on optimizing the



**Figure 5.** (a, b) The first two leading EOF modes of observational weekly ECDs during December–March (shading). The contours represent the simultaneous correlation coefficient between these modes and 500 hPa geopotential height (H500) anomalies from observations (contour interval is 0.1 starting at  $\pm 0.2$ ). The explained variance is shown in the upper-right corners. (c, d) Similar to (a) and (b) but contours are the correlation coefficient between H500 anomalies from model hindcasts and the principal components (PCs) obtained from model hindcasts projected onto the observational EOF modes. Results are week 3 hindcasts.

initialization strategy, and on further model improvement. The predictability sources for subseasonal predictions can be loosely grouped into two types. The first is ascribable to intrinsic climate variability and its teleconnections. This variability is typically characterized by recurring and/or quasi-oscillatory features, such as the MJO, North Atlantic Oscillation (NAO), El Niño/Southern Oscillation (ENSO), and Pacific-North America (PNA) pattern (Stan et al., 2017). In the recent decade, the prediction of internal modes, such as that of the MJO (Kim et al., 2018; Lee et al., 2016; Lim et al., 2018; Xiang et al., 2015) and NAO (Lin et al., 2010; Zuo et al., 2016), has achieved substantial progress. The second one is related to the slowly varying processes that may retain initial memory and persist for a relatively long time, such as SST, sea ice, soil moisture, stratosphere-troposphere coupling (Butler et al., 2019; Son et al., 2016), and atmosphere and land coupling (Dirmeyer et al., 2019; Ford et al., 2018).

In the next two subsections, the emphasis is placed on understanding the physical processes behind the variation and prediction of land ECDs. Since large-scale variability is typically more predictable than small-scale events (Vitart et al., 2019), we examine the leading empirical orthogonal function (EOF) modes that account for the largest share of ECD variance in two relatively large domains: the Eurasia continent and the North America continent, respectively.

### 3.2. ECDs in Eurasia

To extract the dominant spatial pattern of the winter ECDs over Eurasia, we perform an EOF analysis of ECDs in the Eurasian continent (Figure 5). The EOF analysis, through identifying the dominant large-scale modes, is also instrumental in detecting the source of predictability. The primary loading of the first EOF (EOF1) mode resides in the region from Europe to northeastern Asia (Figure 5a). The corresponding atmospheric circulation illustrated by the simultaneous correlation with the 500 hPa weekly

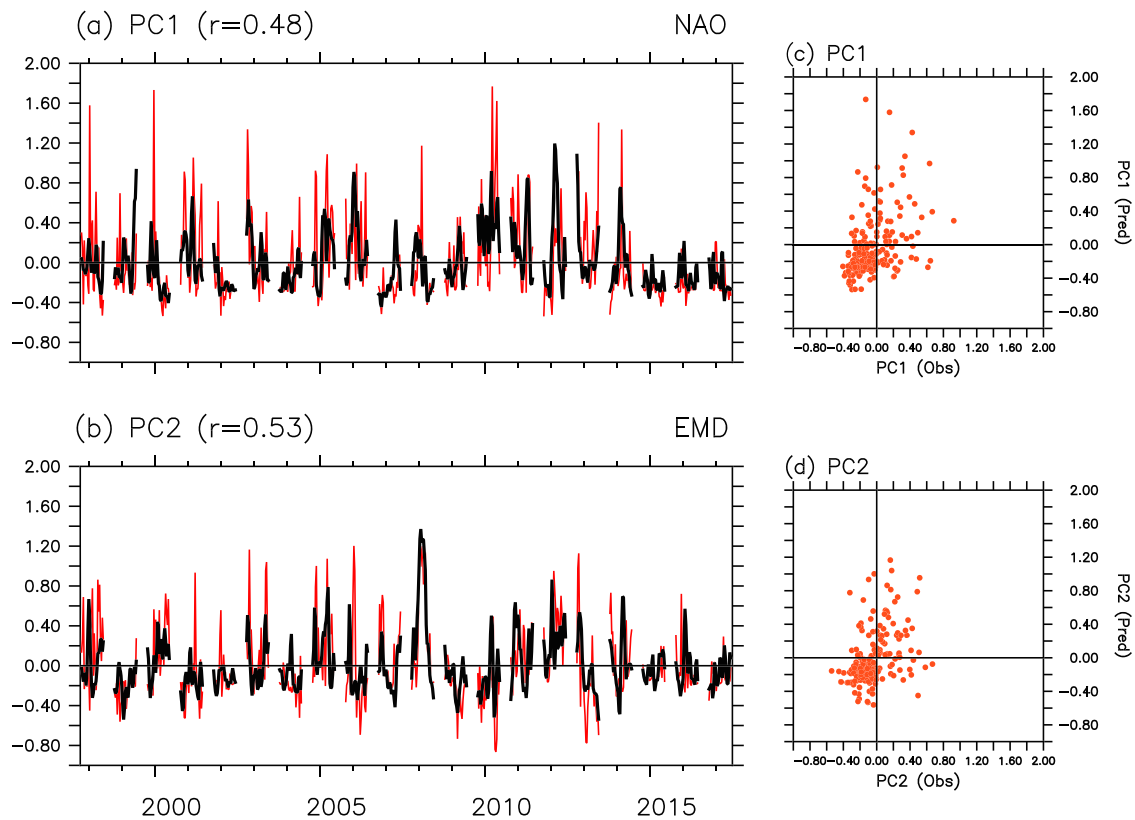


**Figure 6.** The observed (black) and predicted (red) PCs from the (a) first and (b) second leading EOF modes in Eurasia at week 3. The scatter diagram between the observed and predicted (c) PC1 and (d) PC2.

mean geopotential height (H500) anomalies bears a close resemblance to the negative phase of NAO, manifested as above-average H500 centered to the east of Greenland and a southwest-northeast elongated below-average H500 in the midlatitude North Atlantic (Figure 5a). Meanwhile, an anomalous low is present in northeastern Asia as a relatively independent circulation system (Figure 5a). Note that this atmospheric circulation pattern is also strongly related to the Northern Hemisphere land temperature cold extremes on seasonal and long-term trend variability (Johnson et al., 2018).

A similar circulation correlation pattern can be obtained using the extreme H500 days (the frequency of extremely low-pressure) (Figure S2). It suggests that both the reduced weekly mean SAT associated with the Greenland blocking and increased variance associated with the strengthened synoptic eddy activities contribute to the more frequent ECD events in the European continent with the negative phase of NAO (Diao et al., 2014). Note that the negative phase of NAO (blocking) drives the climate system subtly toward a state in which synoptic eddies are favored for a large portion of Europe (their Figure 8a, Diao et al., 2014).

The second EOF mode (EOF2) features salient positive ECD anomalies in a large portion of Asia, with its main action center in southeastern Asia, and weakly negative anomalies to the north (Figure 5b). In association with this mode, the predominance of an anomalous low-pressure system is found in Asia while Europe is dominated by an anomalous high-pressure system. These two modes together account for about 30% of the total variances in the studied domain, and they are likely highly predictable in dynamic models as they are similar to the leading most predictable modes of global SAT anomalies identified solely from a Geophysical Fluid Dynamics Laboratory (GFDL) model (Xiang et al., 2018). Following Xiang et al. (2018), we refer to these two modes as the NAO and Eurasia Meridional Dipole (EMD) mode, respectively.

With the determination of the leading modes, it is therefore essential for models to display skill in predicting these modes to ensure a skillful prediction of ECDs. Figure 6 shows the time series (principal components [PCs]) of these two modes for both observations and week 3 model hindcasts. The correlation coefficients between model hindcasts and observation are 0.48 and 0.53 for these two modes, respectively, both

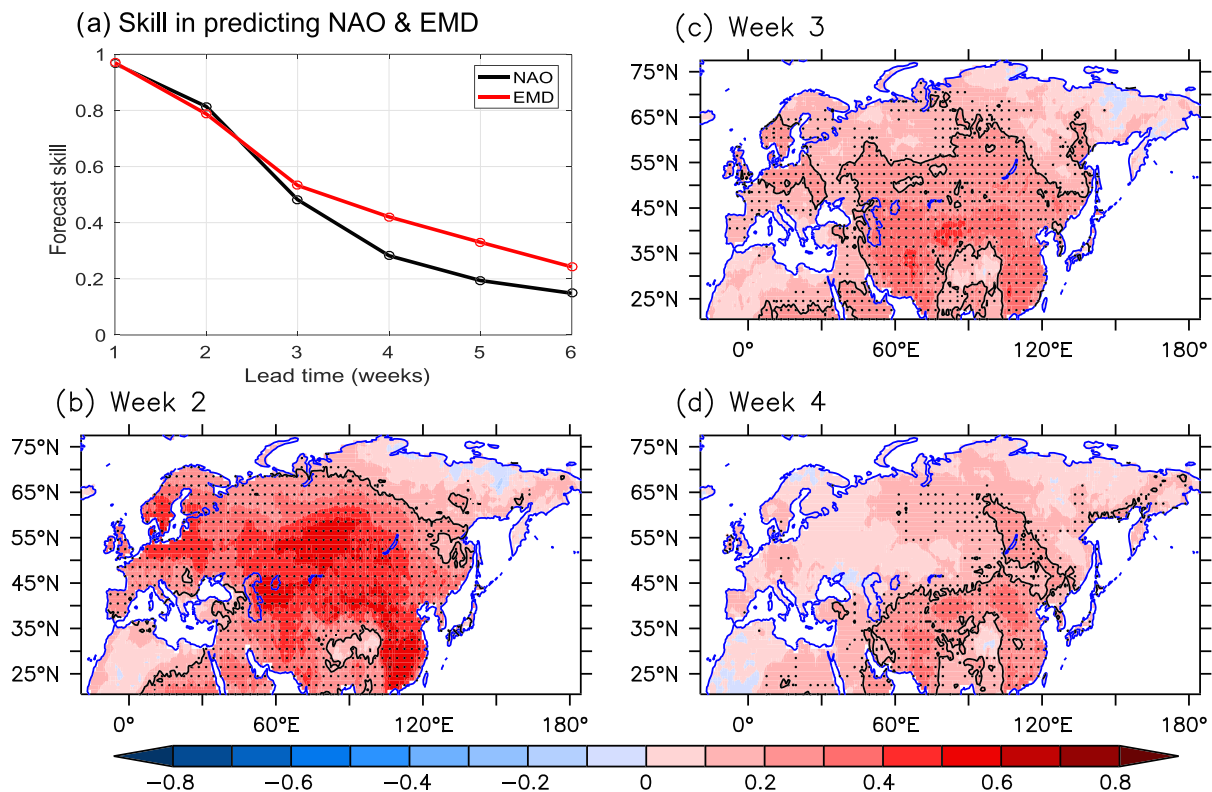


**Figure 7.** (a) The correlation coefficients between the observed and predicted PCs of the first two leading EOF modes as a function of lead time (weeks). The circle indicates that the correlation skill is statistically significant at the 5% level. The (b) week 2, (c) week 3, and (d) week 4 correlation skill using the reconstructed forecast anomalies based on the first two EOF modes in Eurasia.

significant at the 5% level. There is apparent skewness particularly for the NAO mode: The negative phases have smaller magnitude and are less scattered compared to its positive phases, which likely owes to the monopolar nature of the ECD pattern (Figure 5a) and the ECD definition (i.e., below-normal ECDs are bounded by zero). The model has some skill in predicting not only the phases with frequent occurrence of ECDs but also the phases with reduced frequency in ECDs. Both modes show significant correlation skills during the first 6 weeks despite a slightly higher skill in predicting the EMD mode than the NAO mode during week 3 to 6 (Figure 7a).

The forecasted anomalies can be reconstructed using the observed EOF spatial patterns and the projected PCs from model hindcasts (Figures 7b–7d). The anomalies reconstructed from the leading two EOFs show a similar correlation skill with the raw model hindcasts for week 3–4 forecast but a relatively lower skill for week 2 forecast (Figure 7 vs. Figure 3). This confirms that the predictability source for a long-lead prediction mainly originates from the skill in predicting these two leading modes.

Why does the model have skill in predicting these two modes several weeks ahead? One reason we argue is that these modes have dynamically coherent atmospheric circulation patterns so that they potentially have longer persistence than the case with the absence of coherent atmospheric circulations, serving as a source of predictability as for subseasonal forecasting. Note that the model well captures the coupling between the ECD modes and atmospheric circulations, acting as a prerequisite for a skillful subseasonal prediction (Figures 5c and 5d).

There are other sources of predictability related to these two modes. The NAO mode is well described as a Markov (stochastic) process with a timescale of less than 10 days (Feldstein, 2000), and so much of its predictability is rooted in deterministic weather processes. However, several processes are believed to contribute to NAO forecast skill at longer, subseasonal timescales. First, some studies suggest that the NAO is driven partially by the variability of stratospheric polar vortex and its impact sometimes persists for up to

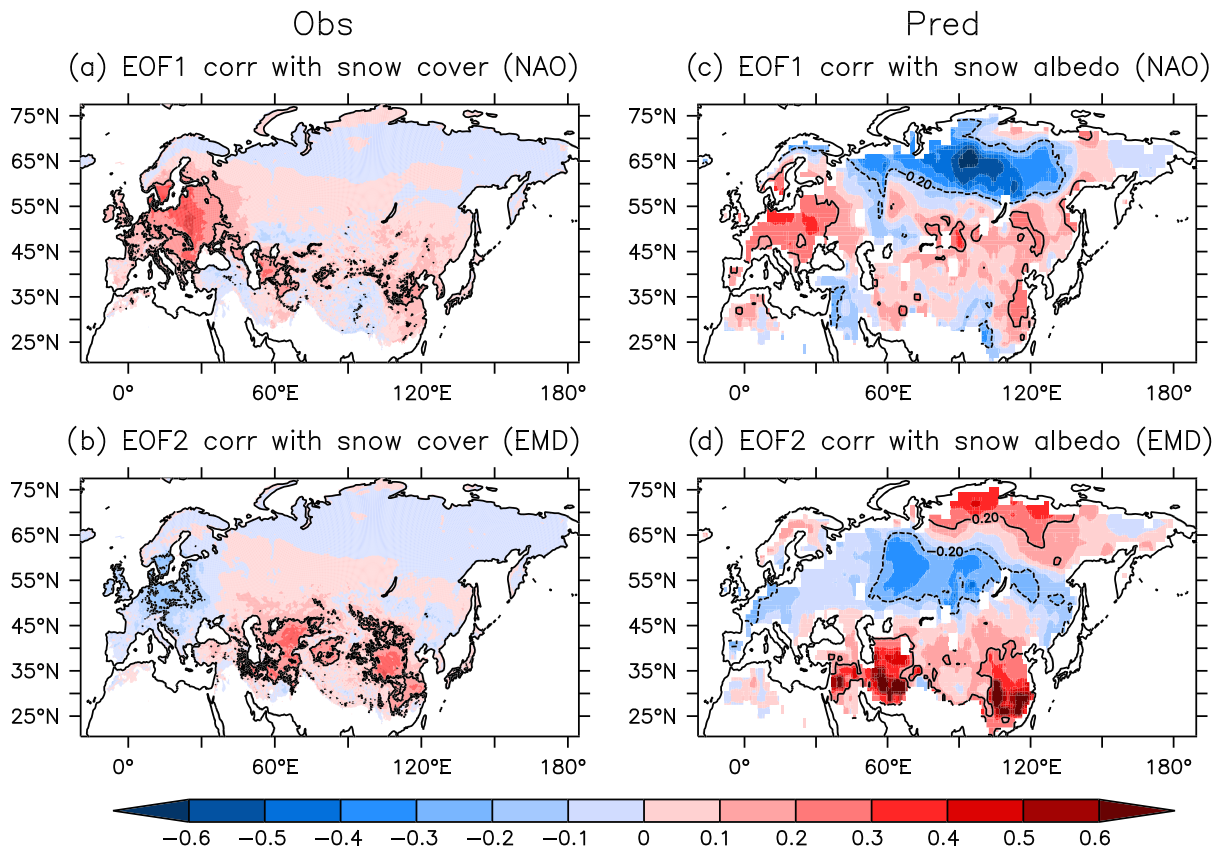


**Figure 8.** (a, b) The simultaneous correlation coefficient between the first two EOF modes in Eurasia and the snow cover anomaly from observations. (c, d) The simultaneous correlation between the PCs of the first two EOF modes in Eurasia and the snow albedo anomaly from model hindcasts. There are differences between observations and model hindcasts evident over Siberia, which is partly due to the different variables used here.

2 months (Baldwin & Dunkerton, 2001; Scaife et al., 2015; Wang et al., 2017; Xiang et al., 2018). Second, some tropical forcings, such as MJO, are able to modulate NAO while its development takes about 5–15 days, contributing to the subseasonal prediction of NAO beyond weather timescale (e.g., Lin et al., 2009). Third, changes in snow cover and snow depth can feed back to affect the NAO circulations and SAT (Dutra et al., 2011; Fletcher et al., 2009), and an improved subseasonal prediction can be achieved with snow initializations (Jeong et al., 2012; Li et al., 2019; Orsolini et al., 2013).

For the NAO mode, a significant correlation with snow cover anomaly is located in Europe but is absent downstream in northern Eurasia (Figure 8a). As northern Eurasia is nearly completely covered by snow in wintertime, the snow depth is also expected to increase associated with this mode, which may reduce the local SAT and increase the chance of occurrence of ECDs (Dutra et al., 2011). For the EMD mode, the high ECD regions generally collocate with the areas with increased snow cover, including some regions in the Middle East and eastern China (Figure 8b). The increased snow cover and a resultant increase in reflection of shortwave radiation act to further reinforce the initial cold SAT anomalies, enhancing the probability of occurrence of extreme events. The snow albedo anomaly from model hindcasts well reproduces the observed snow cover anomaly in observations (Figures 8c and 8d). Note that the snow mass and snow temperature in the ECMWF model are initialized by the Land Data Assimilation System (LDAS); snow albedo and snow density are cycled from the model forecast (<https://confluence.ecmwf.int/display/S2S/ECMWF+Model+Description+CY45R1>).

One remarkable distinction between these two modes is that the atmospheric circulation anomalies for the NAO (EMD) mode are mainly confined to the ocean (land) (Figure 5). For the NAO mode, the atmospheric circulations permit advection of relatively cool and moist air from the ocean to Europe, giving rise to increased snowfall and snow cover. The increased snow cover in Eurasia can likely feed back to influence

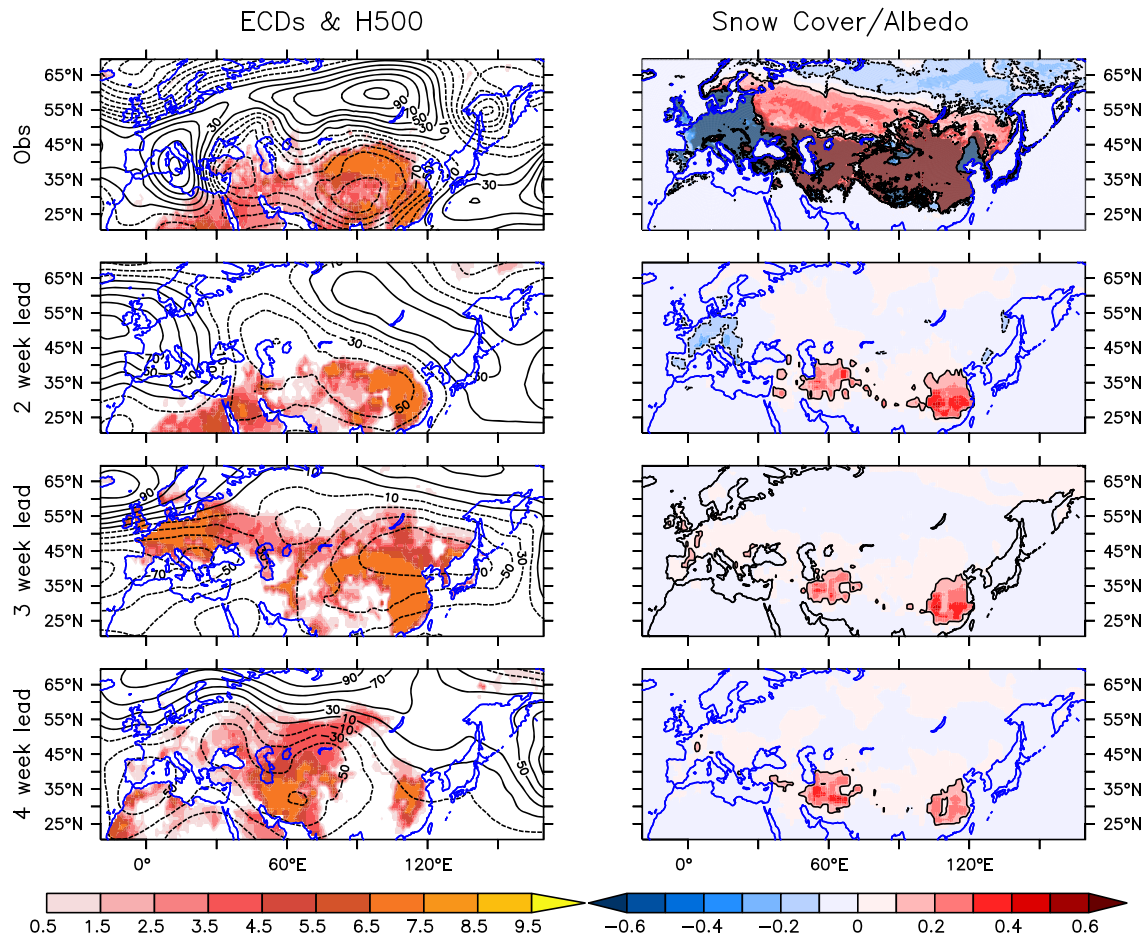


**Figure 9.** The left panel shows the observed and model-predicted (with a lead time of 2, 3, and 4 weeks) ECDs (raw) and H500 (contours, m) anomalies from 28 January 2008 to 3 February 2008 when there is a peak ECD in the southeast China. The right panel shows the corresponding snow cover anomalies from observation and snow albedo anomalies from model hindcasts.

the NAO circulation (Dutra et al., 2011; Fletcher et al., 2009). For the EMD mode, the increased snow cover strengthens the local anomalous low atmospheric circulation system and is conducive to the more frequent occurrence of ECDs. Therefore, we speculate that the EMD mode owes its existence partially to a positive snow-atmosphere circulation feedback mechanism.

We further conducted a case study with prolonged extreme cold events in Southern China and the Middle East from 15 January 2008 to 14 February 2008 (Wen et al., 2009; Zhou et al., 2010) (Figure 9). These 100-year extreme events (i.e., the probability of being equaled or exceeded in a given year is 1%) led to a direct loss of more than \$20 billion associated with the long-lasting extreme cold temperature, excessive snow amount, and severe icing conditions over central and Southern China (Zhou et al., 2010). These events correspond with anomalously high observed PC2 values ( $>0.8$  in Figure 6d). The model well predicts the peak phase of these extreme events in southeast China during 28 January and 3 February, along with its coupled atmospheric circulation and snow changes, with a lead time of 2 to 4 weeks (Figure 9). Both modes experience large, slowly varying interannual variations superimposed on subseasonal variations, and the prediction skill for the above 2008 events is mainly from the skillful prediction of the lower-frequency seasonal persistence (Figure 6).

### 3.3. ECDs in North America

To illustrate the dominant ECD modes in North America, we present, in Figure 10, the first three EOF modes of the observational weekly ECDs. These three modes can explain about 24.9%, 13.1%, and 8.7% of the total variance, respectively. The EOF1 mode is characterized by a rather monopolar structure with its

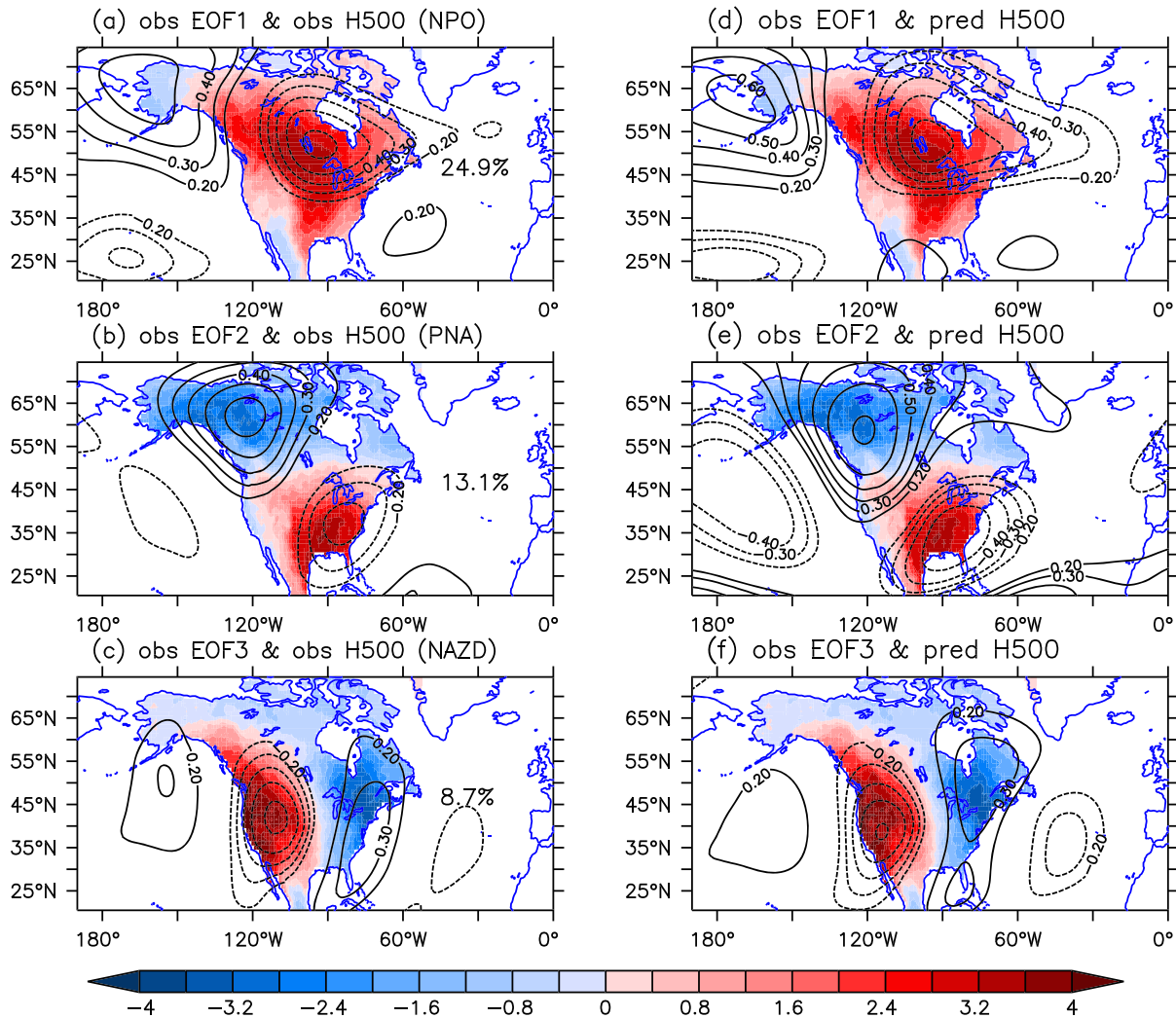


**Figure 10.** Similar to Figure 5 but for the first three leading EOF modes over North America.

maximum over the central continent of North America. Lin et al. (2018) found a similar subseasonal SAT mode by attributing it to northwest-southeast oriented wave train anomalies and the associated southeastward wave activity fluxes. The simultaneous correlation with weekly mean H500 reflects an anomalous high centered in Alaska and an anomalous low covering a large area of northeast America. This resembles a typical pattern of the West Pacific (WP) teleconnection pattern (Wallace & Gutzler, 1981) with its sea level pressure footprint as the North Pacific Oscillation (NPO) mode (Rogers, 1981) (Walker & Bliss, 1932), and also projects onto the so-called East Pacific Oscillation (EPO, <https://www.esrl.noaa.gov/psd/forecasts/forecast2/teleconn/epo.html>). For simplicity, we refer to this mode as the NPO mode hereinafter. The NPO mode was found to be a leading contributor to the wintertime climate anomaly over a large portion of North America (Baxter & Nigam, 2015; Rogers, 1981). In recent decades, North America is more prone to prolonged winter extremes as a consequence of the eastward displacement of the NPO mode (Sung et al., 2019). The NPO mode is likely forced by the meridional migration (equatorward or poleward) of the subtropical jet and the associated eddy activities as found in previous studies (Schubert & Park, 1991; Winters et al., 2019).

The EOF2 mode is characterized by a northwest-southeast dipole pattern (Figure 10b), and the gross features of the associated H500 anomalies are reminiscent of a conventional PNA teleconnection pattern. Previous studies illustrated that the PNA mode can be forced by the migration (extension/retraction and the meridional shift) of the subtropical jet (Schubert & Park, 1991; Winters et al., 2019) and also tropical convective

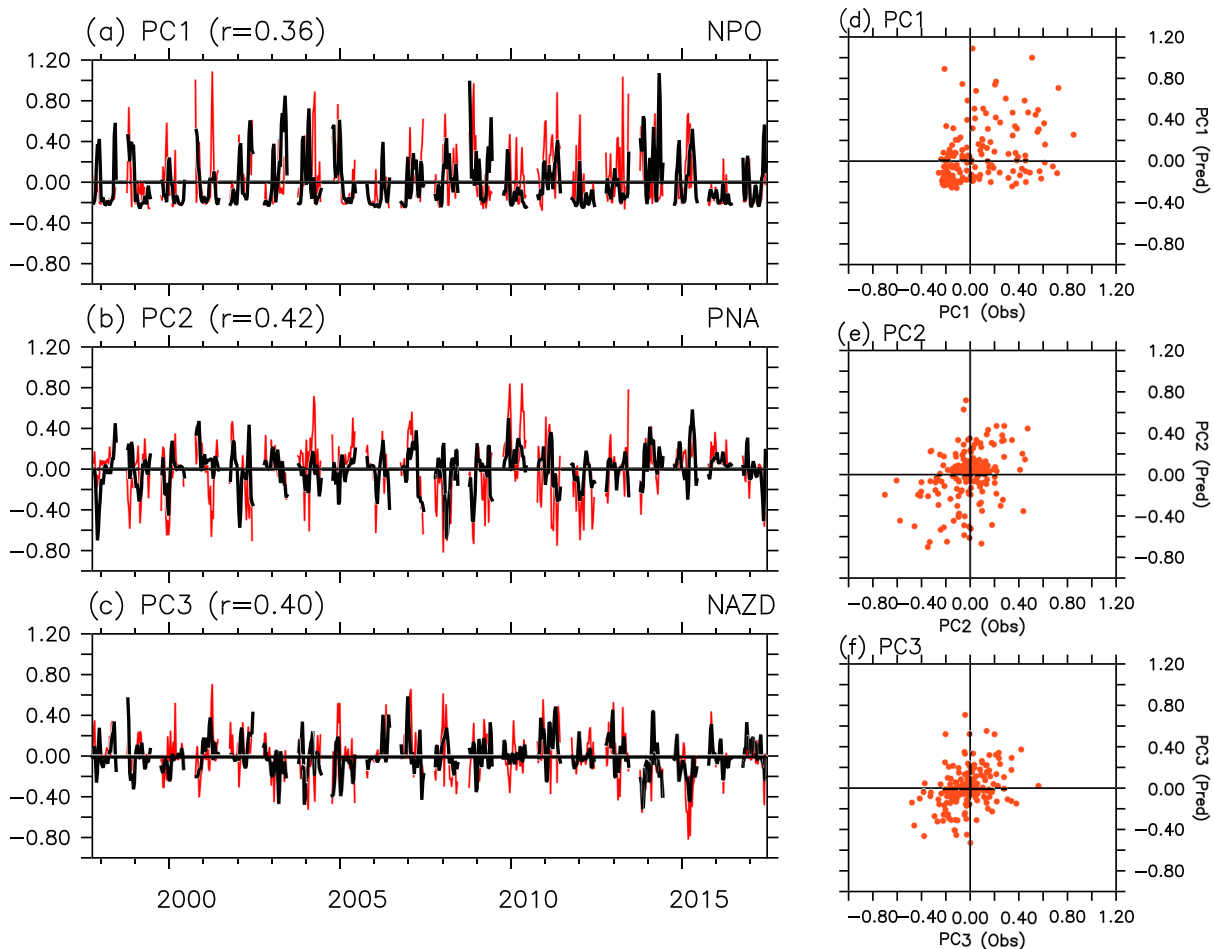


**Figure 11.** Similar to Figure 6 but for the first three leading EOF modes in North America.

perturbations (e.g., Johnson & Feldstein, 2010). The growth and maintenance of the PNA are controlled by the barotropic conversion from the zonally asymmetric mean flow as well as linear dispersion (Feldstein, 2002; Schubert & Park, 1991), and the energy source for PNA is mainly from middle latitudes rather than from the tropics (Schubert & Park, 1991).

The EOF3 mode is manifested as a zonal dipole pattern with enhanced ECDs in western North America and reduced ECDs in northeast North America, accompanied by a zonal wave train atmospheric circulation pattern (Figure 10c). This mode is very similar to one of the weather regimes identified from a cluster analysis (Vigaud et al., 2018), while the detailed mechanisms by which this mode is triggered and maintained remain an open question. The large-scale atmospheric circulation patterns are well simulated in model hindcasts for all three modes (Figures 10d–10f). For simplicity, we refer to these three modes as the NPO, PNA, and the North America Zonal Dipole (NAZD) mode, respectively.

The PCs of these three modes at week 3 are shown in Figure 11. Similar to the NAO mode (Figure 6c), the NPO mode, which also is monopolar, exhibits skewness evident by inspecting Figure 11d. The correlation skill is significant (at the 5% level) but lower in predicting these three modes than the NAO and EMD modes in Eurasia. For these modes, the model fails to predict some of the observed high PC events (highly frequent occurrence of ECDs in some regions) and also forecasts some false alarms (Figures 11d–11f). Further study is required to detail what distinguishes these events from the cases with successful predictions. Investigation of this will be essential to identify the time windows of opportunity for generating useful subseasonal forecasts, in particular for the long-lead weeks 3 to 5 predictions.

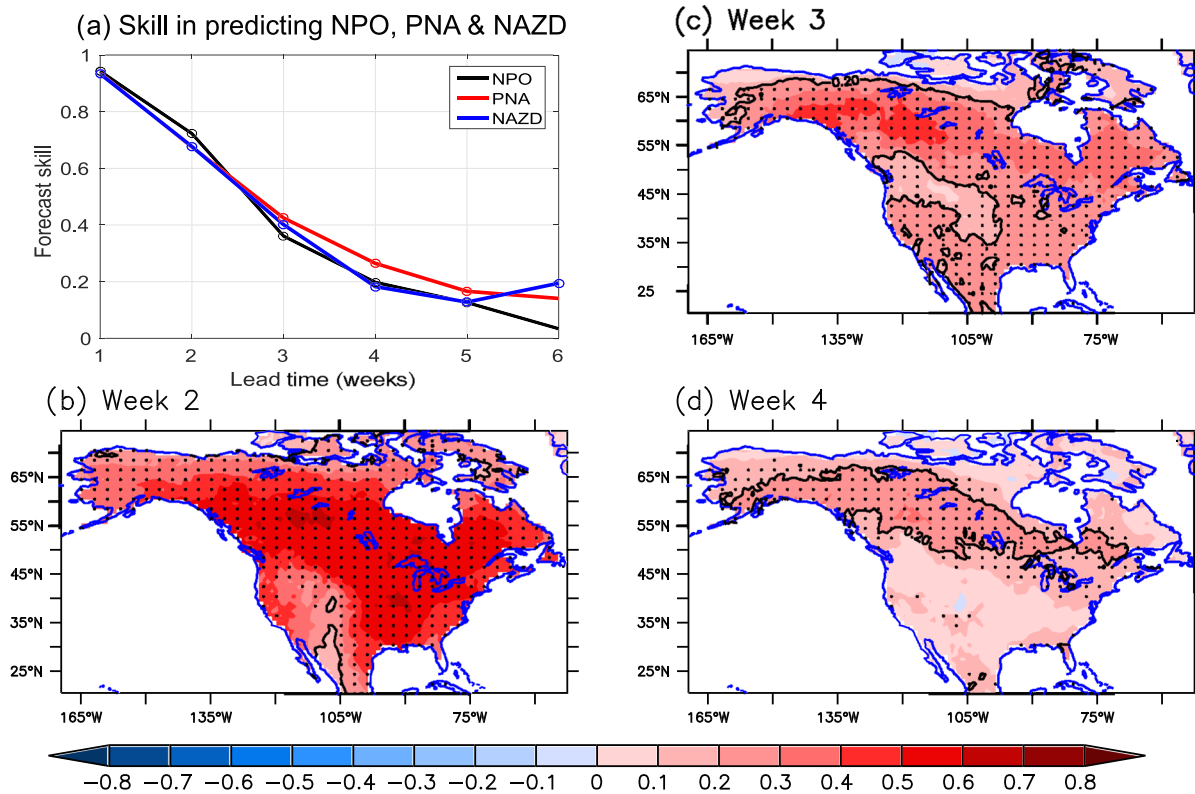


Figure 12. Similar to Figure 7 but using the first three leading EOF modes over North America.

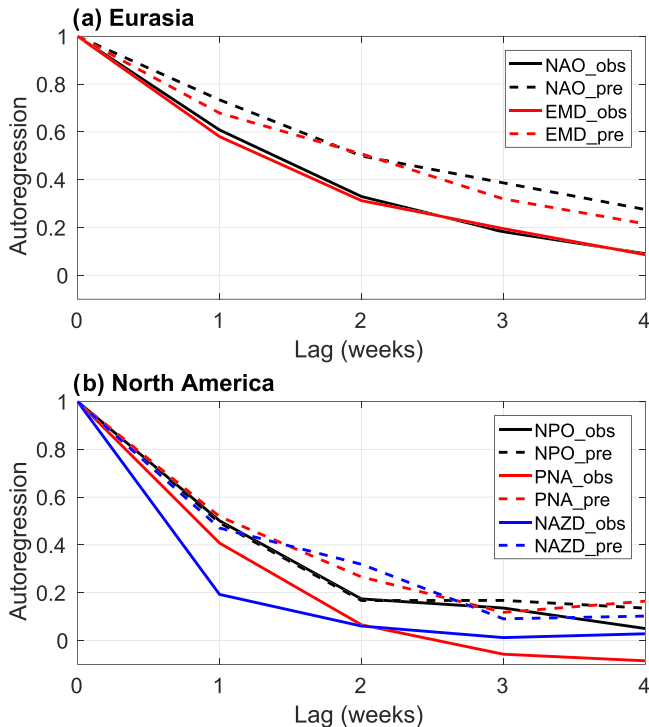


Figure 13. Autoregression functions for the observed (solid) and predicted (dashed) EOF modes in (a) Eurasia and (b) North America.

The ECMWF model shows significant skill in predicting these three modes with a lead time of at least 5 weeks (Figure 12a). The reconstructed hindcast anomalies, based on the three observed EOF spatial patterns and the projected PCs from model hindcasts, yield similar correlation skill as the raw (unfiltered) forecasts (Figures 12b–12d). The skill from reconstructed forecast anomalies is even higher than the raw forecasts for leads of 3–4 weeks. This indicates the prediction skill beyond the weather timescale primarily owes to the skillful prediction of these three modes.

The correlation skill in predicting these three modes is generally lower than that for the first two modes in Eurasia (Figure 12a vs. Figure 7a). One reason is that these three modes decay much faster (weaker persistence) than the NAO and EMD modes in Eurasia (Figure 13). The e-folding timescale of the NAO and EMD mode is about 2 weeks while it is about 1 week for these three modes in North America. Compared to observations, nearly all modes from model hindcasts tend to have longer persistence that is likely due to the fact that the ensemble-mean forecasts have averaged out some of the weather noise (Figure 13).

### 3.4. Domain-Averaged ECD Predictions

The ECD prediction skill is further inspected over four individual domains outlined in Figure 3a. For eastern Asia, the area-mean ECD anomalies show significantly higher correlation skills than the area-mean of the correlation skill (Figure 14). This conclusion is generally valid for other regions (Figures 14b–14d). If the ECD variation

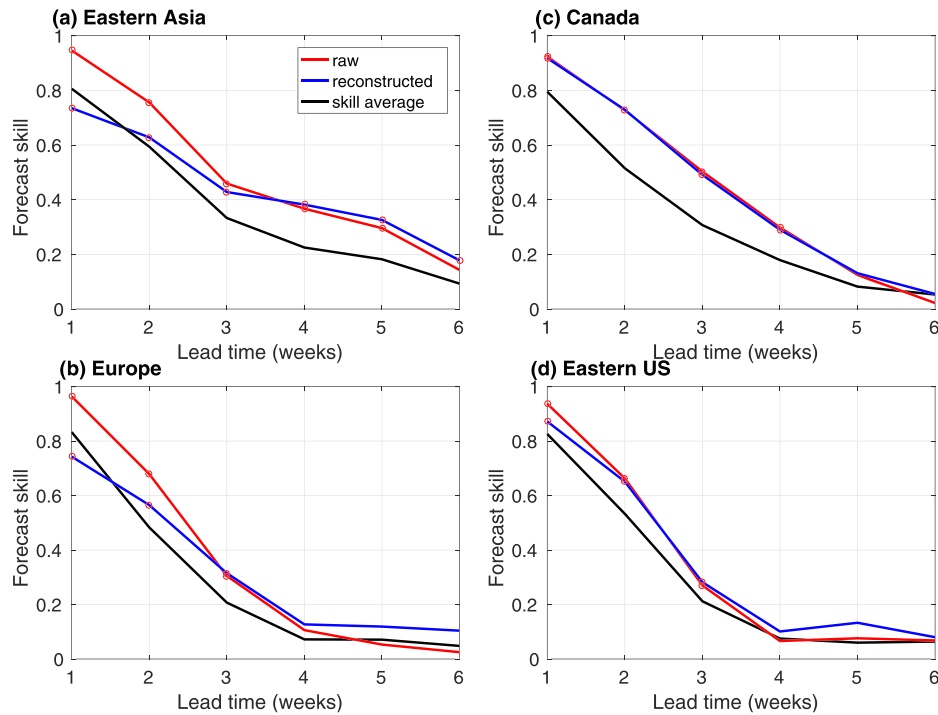


**Figure 14.** The correlation skill for ECDs over (a) Eastern Asia (103E–123E, 20N–45N), (b) Europe (–10–60E, 37–70N), (c) Canada (150W–55W, 50–65N), and (d) Eastern US (100W–60W, 30–43.5E). The individual domains are shown in Figure 3a. The black lines represent the area-mean of correlation coefficients from individual grid points. The red lines are the correlation skill between the area-mean observed and predicted ECD anomalies. The blue lines show the correlation skill between the area-mean observed and predicted ECD anomalies using the reconstructed anomalies based on the first two or three leading EOF modes. The circle indicates that the correlation skill is statistically significant at the 5% level.

in a certain domain is regulated by the same large-scale process, the domain-averaged variation averages out the small-scale noise so that the signal is more pronounced and more predictable than that in an individual grid point. For eastern Asia and Europe, the correlation skill during week 3 and beyond is overall comparable and even higher using the reconstructed hindcast anomalies than the raw hindcasts, supporting the dominance of the leading two modes for subseasonal skill beyond 2 weeks in this region. However, for weeks 1 and 2, the higher-order modes contribute nonnegligible correlation skills, as seen by the higher skill of the raw hindcast data.

Interestingly, the correlation skill is nearly identical between the raw and reconstructed anomalies for Canada and eastern United States (Figures 14c and 14d). This suggests that the predictability sources in North America primarily arise from the prediction of these three modes for both the short to medium-range (weeks 1–2) and subseasonal (week 3 and beyond) predictions. It is also found that the prediction skill is higher in eastern Asia (~5–6 weeks) and northern Canada (~4 weeks), while the skill is generally lower (~3 weeks) for Europe and the eastern United States.

#### 4. Summary and Discussion

Understanding and predicting extremes not only are of paramount interest from a scientific point of view but also have immense direct societal and economic benefits for hazard prevention, effective preparedness, risk management, and even mitigation activities. However, a skillful subseasonal prediction of extremes remains a thorny and challenging issue. Using observations and the ECMWF hindcast data sets, we investigated the mechanisms governing the subseasonal variation of ECDs in boreal wintertime with the aim of gaining insight into its subseasonal predictability. This investigation reveals that the ECMWF model has significant subseasonal prediction skills for weekly ECDs from week 1 to week 3, and the skill can even extend to week 4 for some regions, such as Canada and southeast Asia. For the Eurasian continent, the subseasonal prediction skill mainly originates from the prediction of the two leading modes, the NAO mode and the EMD mode. For

North America, the predictability sources are attributed to the first three modes, the NPO mode, the PNA mode, and the NAZD mode.

The prediction skill of ECDs relies on predicting mean SAT and its synoptic-scale variance. Given its connection with planetary-scale time-mean circulations, the synoptic eddy activities are potentially predictable for a long-lead forecast over some regions, such as Europe (Diao et al., 2014). For all EOF modes, the correlation between the ECDs and mean SAT becomes significantly higher (more negative) for the anomalously strong cases (more frequent occurrence of ECDs) relative to the normal cases (Figures S3 and S4), so that prediction of mean SAT is central to the ECD prediction for the strong anomalies of ECDs.

The subseasonally predictable ECDs are regional manifestations of planetary-scale atmospheric circulations and local boundary (such as snow-atmosphere) feedbacks. The coherent atmospheric circulations facilitate a strengthened and long-lived cold air outbreak, serving as a source of predictability. This study sheds light on the importance of atmospheric internal modes and land-atmosphere coupling on subseasonal predictions. The results support the broad notion that the subseasonal deterministic forecasts have skill for large-scale, long-lasting extreme events but not for some smaller-scale, high-impact events (Vitart et al., 2019). Because we have focused on a single dynamical forecast model in this study, future studies also shall address the degree to which these conclusions apply to other dynamic models as well as the full capability of operational, subseasonal prediction of wintertime extremes.

Whether the subseasonal prediction of extremes is sensitive to particular initial states remains an open question. For example, the cases initialized with negative NAO tend to have high prediction skill for the medium-range forecasts (Ferranti et al., 2015). Observational studies have shown the contribution of MJO on the SAT variability in North America (Hu et al., 2019; Johnson et al., 2013; Schreck et al., 2013; Vecchi & Bond, 2004; Zhou et al., 2012), while its role in the predicting the extratropical SAT is still uncertain (Lin, 2018; Tseng et al., 2018; Xiang et al., 2018). Here we do not specifically elaborate on the relationship between MJO and the EOF modes in the North America, while PNA is more likely to be influenced by the tropical MJO forcing (e.g., Johnson & Feldstein, 2010). Although the importance of tropical and other atmospheric initial states is reserved for future study, the present study provides a point of focus for these forthcoming investigations by determining a small subset of modes that are responsible for nearly all ECD forecast skill over North America and Eurasia for subseasonal lead times beyond 2 weeks.

The seasonal prediction of ECDs has been reported from literature, with very limited prediction skill over land attributed to the prediction of ENSO and climate change (Hamilton et al., 2012; Pepler et al., 2015). It suggests that what is unpredictable at the seasonal timescale becomes predictable at the subseasonal timescale. We also find some significant SST variations associated with the identified modes here, such as the SST tripole in the North Atlantic associated with the NAO mode, and also some local SST signal in the north Pacific related to the NPO mode (not shown). However, we believe the memory and predictability sources for these modes are mainly from the atmosphere and its coupling with the land surface, distinctly different from that for seasonal predictions. Therefore, realistic initial conditions of the atmosphere and land are critical for a skillful subseasonal prediction of ECDs.

### Data Availability Statement

This work is partially based on S2S data sets that are downloaded from the ECMWF server (<https://apps.ecmwf.int/datasets/data/s2s>). The ERA5 data sets are downloaded from <https://cds.climate.copernicus.eu/#!/search?text=ERA5&type=dataset>. The observed snow data sets are downloaded from <https://nsidc.org/data/g02156>. S2S is a joint initiative of the World Weather Research Programme (WWRP) and the World Climate Research Programme (WCRP).

### References

- Baggett, C. F., Barnes, E. A., Maloney, E. D., & Mundhenk, B. D. (2017). Advancing atmospheric river forecasts into subseasonal-to-seasonal time scales. *Geophysical Research Letters*, *44*, 7528–7536. <https://doi.org/10.1002/2017GL074434>
- Baldwin, M. P., & Dunkerton, T. J. (2001). Stratospheric harbingers of anomalous weather regimes. *Science*, *294*(5542), 581–584. <https://doi.org/10.1126/science.1063315>
- Batté, L., Ardilouze, C., & Déqué, M. (2018). Forecasting West African heat waves at subseasonal and seasonal time scales. *Monthly Weather Review*, *146*(3), 889–907. <https://doi.org/10.1175/MWR-D-17-0211.1>

### Acknowledgments

We thank the review comments from Drs. Lucas M. Harris and Gan Zhang as well as three anonymous reviewers. X. J. acknowledges support by the NOAA Climate Program Office under Award NA17OAR4310261.

- Baxter, S., & Nigam, S. (2015). Key role of the North Pacific Oscillation–West Pacific pattern in generating the extreme 2013/14 North American winter. *Journal of Climate*, *28*(20), 8109–8117. <https://doi.org/10.1175/JCLI-D-14-00726.1>
- Bretherton, C. S., Widmann, M., Dymnikov, V. P., Wallace, J. M., & Bladé, I. (1999). The effective number of spatial degrees of freedom of a time-varying field. *Journal of Climate*, *12*(7), 1990–2009. [https://doi.org/10.1175/1520-0442\(1999\)012<1990:TENOSD>2.0.CO;2](https://doi.org/10.1175/1520-0442(1999)012<1990:TENOSD>2.0.CO;2)
- Butler, A., Charlton-Perez, A., Domeisen, D. I. V., Garfinkel, C., Gerber, E. P., Hitchcock, P., et al. (2019). Chapter 11—Sub-seasonal predictability and the stratosphere. In A. W. Robertson & F. Vitart (Eds.), *Sub-seasonal to seasonal prediction* (pp. 223–241). Amsterdam, The Netherlands: Elsevier. <https://doi.org/10.1016/B978-0-12-811714-9.00011-5>
- Cohen, J., Zhang, X., Francis, J., Jung, T., Kwok, R., Overland, J., et al. (2020). Divergent consensus on Arctic amplification influence on midlatitude severe winter weather. *Nature Climate Change*, *10*(1), 20–29. <https://doi.org/10.1038/s41558-019-0662-y>
- Copernicus Climate Change Service (C3S) (2017). ERA5: Fifth generation of ECMWF atmospheric reanalyses of the global climate. Copernicus Climate Change Service Climate Data Store (CDS), date of access. <https://cds.climate.copernicus.eu/cdsapp#!/home>
- de Andrade, F. M., Coelho, C. A. S., & Cavalcanti, I. F. A. (2019). Global precipitation hindcast quality assessment of the subseasonal to seasonal (S2S) prediction project models. *Climate Dynamics*, *52*(9–10), 5451–5475. <https://doi.org/10.1007/s00382-018-4457-z>
- DeFlorio, M. J., Waliser, D. E., Guan, B., Lavers, D. A., Ralph, F. M., & Vitart, F. (2018). Global assessment of atmospheric river prediction skill. *Journal of Hydrometeorology*, *19*(2), 409–426. <https://doi.org/10.1175/JHM-D-17-0135.1>
- Diao, Y., Xie, S.-P., & Luo, D. (2014). Asymmetry of winter European surface air temperature extremes and the North Atlantic Oscillation. *Journal of Climate*, *28*(2), 517–530. <https://doi.org/10.1175/JCLI-D-13-00642.1>
- Dirmeyer, P. A., Gentine, P., Ek, M. B., & Balsamo, G. (2019). Chapter 8—Land surface processes relevant to sub-seasonal to seasonal (S2S) prediction. In A. W. Robertson & F. Vitart (Eds.), *Sub-seasonal to seasonal prediction* (pp. 165–181). Amsterdam, The Netherlands: Elsevier. <https://doi.org/10.1016/B978-0-12-811714-9.00008-5>
- Dutra, E., Schär, C., Viterbo, P., & Miranda, P. M. A. (2011). Land-atmosphere coupling associated with snow cover. *Geophysical Research Letters*, *38*, L15707. <https://doi.org/10.1029/2011GL048435>
- Feldstein, S. B. (2000). The timescale, power spectra, and climate noise properties of teleconnection patterns. *Journal of Climate*, *13*(24), 4430–4440. [https://doi.org/10.1175/1520-0442\(2000\)013<4430:TTPSAC>2.0.CO;2](https://doi.org/10.1175/1520-0442(2000)013<4430:TTPSAC>2.0.CO;2)
- Feldstein, S. B. (2002). Fundamental mechanisms of the growth and decay of the PNA teleconnection pattern. *Quarterly Journal of the Royal Meteorological Society*, *128*(581), 775–796. <https://doi.org/10.1256/0035900021643683>
- Ferranti, L., Corti, S., & Janousek, M. (2015). Flow-dependent verification of the ECMWF ensemble over the Euro-Atlantic sector. *Quarterly Journal of the Royal Meteorological Society*, *141*(688), 916–924. <https://doi.org/10.1002/qj.2411>
- Fletcher, C. G., Hardiman, S. C., Kushner, P. J., & Cohen, J. (2009). The dynamical response to snow cover perturbations in a large ensemble of atmospheric GCM integrations. *Journal of Climate*, *22*(5), 1208–1222. <https://doi.org/10.1175/2008JCLI2505.1>
- Ford, T. W., Dirmeyer, P. A., & Benson, D. O. (2018). Evaluation of heat wave forecasts seamlessly across subseasonal timescales. *npj Climate and Atmospheric Science*, *1*(1), 20. <https://doi.org/10.1038/s41612-018-0027-7>
- Gao, K., Chen, J.-H., Harris, L., Sun, Y., & Lin, S.-J. (2019). Skillful prediction of monthly major hurricane activity in the North Atlantic with two-way nesting. *Geophysical Research Letters*, *46*, 9222–9230. <https://doi.org/10.1029/2019GL083526>
- Gong, D.-Y., & Ho, C.-H. (2004). Intra-seasonal variability of wintertime temperature over East Asia. *International Journal of Climatology*, *24*(2), 131–144. <https://doi.org/10.1002/joc.1006>
- Hamilton, E., Eade, R., Graham, R. J., Scaife, A. A., Smith, D. M., Maidens, A., & MacLachlan, C. (2012). Forecasting the number of extreme daily events on seasonal timescales. *Journal of Geophysical Research*, *117*, D03114. <https://doi.org/10.1029/2011JD016541>
- Hu, W., Liu, P., Zhang, Q., & He, B. (2019). Dominant patterns of winter-time intraseasonal surface air temperature over the CONUS in response to MJO convections. *Climate Dynamics*, *53*(7–8), 3917–3936. <https://doi.org/10.1007/s00382-019-04760-x>
- Jeong, J.-H., Ho, C.-H., Kim, B.-M., & Kwon, W.-T. (2005). Influence of the Madden-Julian Oscillation on wintertime surface air temperature and cold surges in East Asia. *Journal of Geophysical Research*, *110*, D11104. <https://doi.org/10.1029/2004JD005408>
- Jeong, J.-H., Linderholm, H. W., Woo, S.-H., Folland, C., Kim, B.-M., Kim, S.-J., & Chen, D. (2012). Impacts of snow initialization on subseasonal forecasts of surface air temperature for the cold season. *Journal of Climate*, *26*(6), 1956–1972. <https://doi.org/10.1175/JCLI-D-12-00159.1>
- Jiang, X., Xiang, B., Zhao, M., Li, T., Lin, S.-J., Wang, Z., & Chen, J.-H. (2018). Intraseasonal tropical cyclogenesis prediction in a global coupled model system. *Journal of Climate*, *31*(15), 6209–6227. <https://doi.org/10.1175/JCLI-D-17-0454.1>
- Johnson, N. C., Collins, D. C., Feldstein, S. B., L'Heureux, M. L., & Riddle, E. E. (2013). Skillful wintertime North American temperature forecasts out to 4 weeks based on the state of ENSO and the MJO. *Weather and Forecasting*, *29*(1), 23–38. <https://doi.org/10.1175/WAF-D-13-00102.1>
- Johnson, N. C., & Feldstein, S. B. (2010). The continuum of North Pacific sea level pressure patterns: Intraseasonal, interannual, and interdecadal variability. *Journal of Climate*, *23*(4), 851–867. <https://doi.org/10.1175/2009JCLI3099.1>
- Johnson, N. C., Xie, S.-P., Kosaka, Y., & Li, X. (2018). Increasing occurrence of cold and warm extremes during the recent global warming slowdown. *Nature Communications*, *9*(1), 1724. <https://doi.org/10.1038/s41467-018-04040-y>
- Kim, H., Vitart, F., & Waliser, D. E. (2018). Prediction of the Madden–Julian Oscillation: A review. *Journal of Climate*, *31*(23), 9425–9443. <https://doi.org/10.1175/JCLI-D-18-0210.1>
- Lee, C.-Y., Camargo, S. J., Vitart, F., Sobel, A. H., & Tippett, M. K. (2018). Subseasonal tropical cyclone genesis prediction and MJO in the S2S dataset. *Weather and Forecasting*, *33*(4), 967–988. <https://doi.org/10.1175/WAF-D-17-0165.1>
- Lee, J.-Y., Fu, X., & Wang, B. (2016). Predictability and prediction of the Madden-Julian Oscillation: A review on progress and current status. In *The global monsoon system* (pp. 147–159). Singapore: World Scientific. [https://doi.org/10.1142/9789813200913\\_0012](https://doi.org/10.1142/9789813200913_0012)
- Lee, S.-S., Moon, J.-Y., Wang, B., & Kim, H.-J. (2017). Subseasonal prediction of extreme precipitation over Asia: Boreal summer intraseasonal oscillation perspective. *Journal of Climate*, *30*(8), 2849–2865. <https://doi.org/10.1175/JCLI-D-16-0206.1>
- Li, F., Orsolini, Y. J., Keenlyside, N., Shen, M. L., Counillon, F., & Wang, Y. G. (2019). Impact of snow initialization in subseasonal-to-seasonal winter forecasts with the Norwegian climate prediction model. *Journal of Geophysical Research: Atmospheres*, *124*, 10,033–10,048. <https://doi.org/10.1029/2019JD030903>
- Liang, P., Lin, H., & Ding, Y. (2018). Dominant modes of subseasonal variability of East Asian summertime surface air temperature and their predictions. *Journal of Climate*, *31*(7), 2729–2743. <https://doi.org/10.1175/JCLI-D-17-0368.1>
- Lim, Y., Son, S.-W., & Kim, D. (2018). MJO prediction skill of the subseasonal-to-seasonal prediction models. *Journal of Climate*, *31*(10), 4075–4094. <https://doi.org/10.1175/JCLI-D-17-0545.1>
- Lin, H. (2018). Predicting the dominant patterns of subseasonal variability of wintertime surface air temperature in extratropical northern hemisphere. *Geophysical Research Letters*, *45*, 4381–4389. <https://doi.org/10.1029/2018GL077509>

- Lin, H., Brunet, G., & Derome, J. (2009). An observed connection between the North Atlantic Oscillation and the Madden-Julian Oscillation. *Journal of Climate*, *22*(2), 364–380. <https://doi.org/10.1175/2008JCLI2515.1>
- Lin, H., Brunet, G., & Fontecilla, J. S. (2010). Impact of the Madden-Julian Oscillation on the intraseasonal forecast skill of the North Atlantic Oscillation. *Geophysical Research Letters*, *37*, L19803. <https://doi.org/10.1029/2010GL044315>
- Lin, H., Mo, R., Vitart, F., & Stan, C. (2018). Eastern Canada flooding 2017 and its subseasonal predictions. *Atmosphere-Ocean*, *57*(3), 195–207. <https://doi.org/10.1080/07055900.2018.1547679>
- Luo, X., & Wang, B. (2017). How predictable is the winter extremely cold days over temperate East Asia? *Climate Dynamics*, *48*(7–8), 2557–2568. <https://doi.org/10.1007/s00382-016-3222-4>
- Mariotti, A., Ruti, P. M., & Rixen, M. (2018). Progress in subseasonal to seasonal prediction through a joint weather and climate community effort. *npj Climate and Atmospheric Science*, *1*(1), 4. <https://doi.org/10.1038/s41612-018-0014-z>
- Mundhenk, B. D., Barnes, E. A., Maloney, E. D., & Baggett, C. F. (2018). Skillful empirical subseasonal prediction of landfalling atmospheric river activity using the Madden-Julian oscillation and quasi-biennial oscillation. *npj Climate and Atmospheric Science*, *1*(1), 20177. <https://doi.org/10.1038/s41612-017-0008-2>
- National Ice Center (2008). updated daily. IMS Daily Northern Hemisphere Snow and Ice Analysis at 1 km, 4 km, and 24 km Resolutions, Version 1. (Indicate subset used). Boulder, Colorado USA. NSIDC: National Snow and Ice Data Center. <https://doi.org/10.7265/N52R3PMC>. (Date Accessed).
- Orsolini, Y. J., Senan, R., Balsamo, G., Doblas-Reyes, F. J., Vitart, F., Weisheimer, A., et al. (2013). Impact of snow initialization on sub-seasonal forecasts. *Climate Dynamics*, *41*(7–8), 1969–1982. <https://doi.org/10.1007/s00382-013-1782-0>
- Park, T.-W., Ho, C.-H., Jeong, S.-J., Choi, Y.-S., Park, S. K., & Song, C.-K. (2011). Different characteristics of cold day and cold surge frequency over East Asia in a global warming situation. *Journal of Geophysical Research*, *116*, D12118. <https://doi.org/10.1029/2010JD015369>
- Pegion, K., Kirtman, B. P., Becker, E., Collins, D. C., LaJoie, E., Burgman, R., et al. (2019). The Subseasonal Experiment (SubX): A multi-model subseasonal prediction experiment. *Bulletin of the American Meteorological Society*, *100*(10), 2043–2060. <https://doi.org/10.1175/BAMS-D-18-0270.1>
- Pepler, A. S., Díaz, L. B., Prodhomme, C., Doblas-Reyes, F. J., & Kumar, A. (2015). The ability of a multi-model seasonal forecasting ensemble to forecast the frequency of warm, cold and wet extremes. *Weather and Climate Extremes*, *9*, 68–77. <https://doi.org/10.1016/j.wace.2015.06.005>
- Rogers, J. C. (1981). The North Pacific Oscillation. *Journal of Climatology*, *1*(1), 39–57. <https://doi.org/10.1002/joc.3370010106>
- Scaife, A. A., Karpechko, A. Y., Baldwin, M. P., Brookshaw, A., Butler, A. H., Eade, R., et al. (2015). Seasonal winter forecasts and the stratosphere. *Atmospheric Science Letters*, *17*(1), 51–56. <https://doi.org/10.1002/asl.598>
- Schreck, C. J., Cordeira, J. M., & Margolin, D. (2013). Which MJO events affect North American temperatures? *Monthly Weather Review*, *141*(11), 3840–3850. <https://doi.org/10.1175/MWR-D-13-00118.1>
- Schubert, S. D., & Park, C.-K. (1991). Low-frequency intraseasonal tropical-extratropical interactions. *Journal of the Atmospheric Sciences*, *48*(4), 629–650. [https://doi.org/10.1175/1520-0469\(1991\)048<0629:LFITEI>2.0.CO;2](https://doi.org/10.1175/1520-0469(1991)048<0629:LFITEI>2.0.CO;2)
- Son, S.-W., Lim, Y., Yoo, C., Hendon, H. H., & Kim, J. (2016). Stratospheric control of the Madden-Julian Oscillation. *Journal of Climate*, *30*(6), 1909–1922. <https://doi.org/10.1175/JCLI-D-16-0620.1>
- Stan, C., Straus, D. M., Frederiksen, J. S., Lin, H., Maloney, E. D., & Schumacher, C. (2017). Review of tropical-extratropical teleconnections on intraseasonal time scales. *Reviews of Geophysics*, *55*, 902–937. <https://doi.org/10.1002/2016RG000538>
- Sung, M.-K., Jang, H.-Y., Kim, B.-M., Yeh, S.-W., Choi, Y.-S., & Yoo, C. (2019). Tropical influence on the North Pacific Oscillation drives winter extremes in North America. *Nature Climate Change*, *9*(5), 413–418. <https://doi.org/10.1038/s41558-019-0461-5>
- Tseng, K. C., Barnes, E. A., & Maloney, E. D. (2018). Prediction of the midlatitude response to strong Madden-Julian Oscillation events on S2S time scales. *Geophysical Research Letters*, *45*, 463–470. <https://doi.org/10.1002/2017GL075734>
- Vecchi, G. A., & Bond, N. A. (2004). The Madden-Julian Oscillation (MJO) and northern high latitude wintertime surface air temperatures. *Geophysical Research Letters*, *31*, L04104. <https://doi.org/10.1029/2003GL018645>
- Vigaud, N., Robertson, A. W., & Tippett, M. K. (2018). Predictability of recurrent weather regimes over North America during winter from submonthly reforecasts. *Monthly Weather Review*, *146*(8), 2559–2577. <https://doi.org/10.1175/MWR-D-18-0058.1>
- Vitart, F., et al. (2016). The subseasonal to seasonal (S2S) prediction project database. *Bulletin of the American Meteorological Society*, *98*(1), 163–173. <https://doi.org/10.1175/BAMS-D-16-0017.1>
- Vitart, F., Cunningham, C., DeFlorio, M., Dutra, E., Ferranti, L., Golding, B., et al. (2019). Sub-seasonal to seasonal prediction of weather extremes. In A. W. Robertson & F. Vitart (Eds.), *Sub-seasonal to seasonal prediction, 978-0-12-811714-9*. Amsterdam, The Netherlands: Elsevier. <https://doi.org/10.1016/B978-0-12-811714-9.00017-6>
- Walker, G. T., & Bliss, E. W. (1932). Memoirs of the Royal Meteorological Society. *World Weather V*, *4*, 53–84.
- Wallace, J. M., & Gutzler, D. S. (1981). Teleconnections in the geopotential height field during the northern hemisphere winter. *Monthly Weather Review*, *109*(4), 784–812. [https://doi.org/10.1175/1520-0493\(1981\)109<0784:TITGHF>2.0.CO;2](https://doi.org/10.1175/1520-0493(1981)109<0784:TITGHF>2.0.CO;2)
- Wang, L., Ting, M., & Kushner, P. J. (2017). A robust empirical seasonal prediction of winter NAO and surface climate. *Scientific Reports*, *7*(1), 279. <https://doi.org/10.1038/s41598-017-00353-y>
- Wayand, N. E., Bitz, C. M., & Blanchard-Wrigglesworth, E. (2019). A year-round subseasonal-to-seasonal sea ice prediction portal. *Geophysical Research Letters*, *46*, 3298–3307. <https://doi.org/10.1029/2018GL081565>
- Wen, M., Yang, S., Kumar, A., & Zhang, P. (2009). An analysis of the large-scale climate anomalies associated with the snowstorms affecting China in January 2008. *Monthly Weather Review*, *137*(3), 1111–1131. <https://doi.org/10.1175/2008MWR2638.1>
- White, C. J., Carlsen, H., Robertson, A. W., Klein, R. J. T., Lazo, J. K., Kumar, A., et al. (2017). Potential applications of subseasonal-to-seasonal (S2S) predictions. *Meteorological Applications*, *24*(3), 315–325. <https://doi.org/10.1002/met.1654>
- Winters, A. C., Keyser, D., & Bosart, L. F. (2019). The development of the North Pacific jet phase diagram as an objective tool to monitor the state and forecast skill of the upper-tropospheric flow pattern. *Weather and Forecasting*, *34*(1), 199–219. <https://doi.org/10.1175/WAF-D-18-0106.1>
- Xiang, B., Lin, S.-J., Zhao, M., Johnson, N. C., Yang, X., & Jiang, X. (2018). Subseasonal week 3–5 surface air temperature prediction during boreal wintertime in a GFDL model. *Geophysical Research Letters*, *46*, 416–425. <https://doi.org/10.1029/2018GL081314>
- Xiang, B., Lin, S.-J., Zhao, M., Zhang, S., Vecchi, G., Li, T., et al. (2014). Beyond weather time-scale prediction for Hurricane Sandy and Super Typhoon Haiyan in a global climate model. *Monthly Weather Review*, *143*(2), 524–535. <https://doi.org/10.1175/MWR-D-14-00227.1>
- Xiang, B., Zhao, M., Jiang, X., Lin, S.-J., Li, T., Fu, X., & Vecchi, G. (2015). The 3–4-week MJO prediction skill in a GFDL coupled model. *Journal of Climate*, *28*(13), 5351–5364. <https://doi.org/10.1175/JCLI-D-15-0102.1>

- Yang, X., Rosati, A., Zhang, S., Delworth, T. L., Gudgel, R. G., Zhang, R., et al. (2012). A predictable AMO-like pattern in the GFDL fully coupled ensemble initialization and decadal forecasting system. *Journal of Climate*, *26*(2), 650–661. <https://doi.org/10.1175/JCLI-D-12-00231.1>
- Yoo, C., Johnson, N. C., Chang, C.-H., Feldstein, S. B., & Kim, Y.-H. (2018). Subseasonal prediction of wintertime east Asian temperature based on atmospheric teleconnections. *Journal of Climate*, *31*(22), 9351–9366. <https://doi.org/10.1175/JCLI-D-17-0811.1>
- Zampieri, L., Goessling, H. F., & Jung, T. (2018). Bright prospects for Arctic Sea ice prediction on subseasonal time scales. *Geophysical Research Letters*, *45*, 9731–9738. <https://doi.org/10.1029/2018GL079394>
- Zhou, B., Gu, L., Ding, Y., Shao, L., Wu, Z., Yang, X., et al. (2010). The great 2008 Chinese ice storm: Its socioeconomic–ecological impact and sustainability lessons learned. *Bulletin of the American Meteorological Society*, *92*(1), 47–60. <https://doi.org/10.1175/2010BAMS2857.1>
- Zhou, S., L'Heureux, M., Weaver, S., & Kumar, A. (2012). A composite study of the MJO influence on the surface air temperature and precipitation over the Continental United States. *Climate Dynamics*, *38*(7-8), 1459–1471. <https://doi.org/10.1007/s00382-011-1001-9>
- Zuo, J., Ren, H.-L., Wu, J., Nie, Y., & Li, Q. (2016). Subseasonal variability and predictability of the Arctic Oscillation/North Atlantic Oscillation in BCC\_AGCM2.2. *Dynamics of Atmospheres and Oceans*, *75*, 33–45. <https://doi.org/10.1016/j.dynatmoce.2016.05.002>